HHS Public Access

Author manuscript

Annu Int Conf IEEE Eng Med Biol Soc. Author manuscript; available in PMC 2022 March 17.

Published in final edited form as:

Annu Int Conf IEEE Eng Med Biol Soc. 2021 November ; 2021: 2668–2671. doi:10.1109/EMBC46164.2021.9630246.

Electric Source Imaging on Intracranial EEG Localizes Spatiotemporal Propagation of Interictal Spikes in Children with Epilepsy

Margherita A.G. Matarrese,
Unit of Non-Linear Physics and Mathematical Modeling, Engineering Department, Università Campus Bio-Medico di Roma, Rome, Italy; Jane and John Justin Neurosciences Center, Cook Children's Health Care System, Fort Worth, TX, USA.

Alessandro Loppini,
Unit of Non-Linear Physics and Mathematical Modeling, Engineering Department, Università Campus Bio-Medico di Roma, Rome, Italy

Saeed Jahromi,
Jane and John Justin Neurosciences Center, Cook Children's Health Care System, Fort Worth, TX, USA.; Department of Bioengineering, University of Texas at Arlington, Arlington, TX, USA

Eleonora Tamilia,
Boston Children's Hospital, Harvard Medical School, Boston, MA, USA

Lorenzo Fabbri,
Jane and John Justin Neurosciences Center, Cook Children's Health Care System, Fort Worth, TX, USA.; Department of Bioengineering, University of Texas at Arlington, Arlington, TX, USA

Joseph R. Madsen,
Boston Children's Hospital, Harvard Medical School, Boston, MA, USA

Phillip L. Pearl,
Boston Children's Hospital, Harvard Medical School, Boston, MA, USA

Simonetta Filippi,
Unit of Non-Linear Physics and Mathematical Modeling, Engineering Department, Università Campus Bio-Medico di Roma, Rome, Italy

Christos Papadelis
Jane and John Justin Neurosciences Center, Cook Children's Health Care System, Fort Worth, TX, USA.; Department of Bioengineering, University of Texas at Arlington, Arlington, TX, USA; Boston Children's Hospital, Harvard Medical School, Boston, MA, USA; School of Medicine, Texas Christian University and University of North Texas Health Science Center, Fort Worth, TX, USA.

Abstract

*Corresponding author: christos.papadelis@cookchildrens.org.

Interictal epileptiform discharges (IEDs) serve as sensitive but not specific biomarkers of epilepsy that can delineate the epileptogenic zone (EZ) in patients with drug resistant epilepsy (DRE) undergoing surgery. Intracranial EEG (icEEG) studies have shown that IEDs propagate in time across large areas of the brain. The onset of this propagation is regarded as a more specific biomarker of epilepsy than areas of spread. Yet, the limited spatial resolution of icEEG does not allow to identify the onset of this activity with high precision. Here, we propose a new method of mapping the spatiotemporal propagation of IEDs (and identify its onset) by using Electrical Source Imaging (ESI) on icEEG bypassing the spatial limitations of icEEG. We validated our method on icEEG recordings from 8 children with DRE who underwent surgery with good outcome (Engel score = 1). On each icEEG channel, we detected IEDs and identified the propagation onset using an automated algorithm. We localized the propagation of IEDs with dynamic Statistical Parametric Mapping (dSPM) using a time-sliding window approach. We defined two brain regions: the ESI-onset and ESI-spread zone. We estimated the overlap of these regions with resection volume (in percentage), which served as the *gold-standard* of the EZ. We also estimated the mean distance of these regions from resection and clinically defined seizure onset zone (SOZ). We observed spatiotemporal propagation of IEDs in all patients across several channels (98 [85-102]) with a mean duration of 155 ms [96-186 ms]. A higher overlap with resection was seen for the ESI-onset zone compared to spread (73.3 % [47.4-100 %], 36.5 % [20.3-59.9 %], $p = 0.008$). The distance of the ESI-onset from resection was shorter compared to the ESI-spread zone (4.3 mm [3.4-5.5 mm], 7.4 mm [6.0-20.6 mm], $p = 0.008$) and the same trend was observed for the distance from the SOZ (11.9 mm [7.2-15.1 mm], 20.6 mm [15.4-27.2 mm], $p = 0.02$). These findings show that our method can map the spatiotemporal propagation of IEDs and delineate its onset, which is a reliable and focal biomarker of the EZ in children with DRE.

Clinical Relevance ——ESI on icEEG recordings of children with DRE can localize the spikes propagation phenomenon and help in the delineation of the EZ.

I. Introduction

Epilepsy is a common neurological disorder affecting both adults and children. It is an alteration of normal brain functioning caused by a synchronous hyperactivation of a brain region, called epileptogenic zone (EZ) [1]. Antiepileptic medications are the solution for many patients but one third of patients suffer of drug resistant epilepsy (DRE), and continue to have seizures despite the administration of antiepileptic drugs. For these patients, the best option to avoid a life of disability and reach a seizures control is epilepsy surgery. The goal of epilepsy surgery is to resect the EZ without functional and neurological deficit for the patient [2]. To date, there are not clinical exams to unambiguously delineate the EZ, but its localization can only be estimated through various epilepsy biomarkers looking at interictal and ictal period [3].

Concerning the interictal period, the biomarker of epilepsy par excellence is interictal epileptiform discharges (IEDs), or spikes. Yet, IEDs are observed in large areas of the brain that are not purely epileptogenic and their resection do not bring any benefit to the patient. Hence, there is an urgent need to find a more precise biomarker to distinguish epileptogenic areas from healthy brain regions. Numerous studies have investigated the propagation phenomenon of IEDs through electrodes that are invasively implanted into or on

the cortex [4]-[6], noting that the tissue that gives rise to the first spikes, called onset spikes, is more epileptogenic than the tissue where the spikes spread over time. Yet, since invasive electrode implantation does not provide full coverage of the brain volume and each electrode is several mm to one cm away from its neighbors, current methodological approaches are unable to map the extent of the spike propagation phenomenon and finely identify its onset. As already demonstrated in various studies. Electric Source Imaging (ESI) can be a useful tool to overcome these limitations, proving new clinical information about how and where electric signals are generated into the brain [7]-[10].

Here, we propose a new method of mapping the spatiotemporal propagation of IEDs (and identify its onset) by using ESI on icEEG bypassing the spatial limitations of icEEG. We validated our method on icEEG recordings from children with DRE who underwent surgery with a good surgical outcome (Engel score = 1). This tool could bring an undoubted benefit in the pre-surgical planning of patients with DRE because it would allow a more focal definition of the EZ used by clinicians.

II. Methodology

A. Patients cohort

In this retrospective study, eight patients with DRE who had a resective surgery after long-term icEEG monitoring (LTM with icEEG) at Epilepsy Center of Boston Children's Hospital between July 2012 and May 2016, were included (see Table I). These patients were included because they met the following inclusion criteria: (i) LTM with icEEG (grid, strips and/or depth electrodes); (ii) availability of high resolution pre-surgical MRI and post-implantation computerized tomography (CT); (iii) precise information on resection and Seizure Onset Zone (SOZ); and (iv) good surgical outcome, i.e. the patient is seizure free after surgery, at least one year after surgery. Only patients with an obvious spike propagation in >3 channels seen with visual inspection in icEEG recordings (windows of 10 s in average montage with signal band-pass filtered between 1-70 Hz) were considered. Institutional Review Board of BCH approved this study protocol (IRB117 P00022114), without informed consent due to the retrospective nature of the study.

B. Long-term intracranial EEG monitoring

Invasive monitoring (also known as Phase 2) with subdural and/or depth electrodes was performed with the XLTEK NeuroWorks (Natus Inc., USA) recording system for several days with a sampling frequency of 2 kHz. The number, location and type of electrodes were decided by clinicians after the non-invasive Phase I of pre-surgical evaluation. Subdural grid and strip electrodes (Ad-Tech., USA) had a diameter of 2.3 mm with a distance between them of 10 mm while depth electrodes (Ad-Tech., USA) had 10 linearly arranged contacts with a diameter of 1.1 mm and an inter-distance of 3-5 mm.

C. Electrodes locations: brain shift problem resolution with pre-operative MRI and post-implant CT

To determine the anatomical location of icEEG contacts, we performed a co-registration between the post-implant CT (voxel size = $0.5 \times 0.5 \times 0.5$ mm^3) scan and the pre-

operative MRIs using *Brainstorm* [11]. Pre-operative anatomical MRI was acquired with magnetization-prepared rapid acquisition gradient-echo sequences (MPRAGE; TE = 1.74 ms, TR = 2, 540 ms voxel size = 1 × 1 × 1 mm^3) using a high resolution 3T scanner (TIM TRIO, Siemens AG, Erlangen, Germany) [12]. Each intracranial contact location was firstly established by manual co-registration with CT-MRI images (Fig. 1B). Subdural electrodes were then projected on the 3D patient's specific model of cortex, reconstructed with *FreeSurfer* [13] starting from the preoperative MRI, to compensate the brain shift caused by the surgical implantation (Fig. 1C). When depth electrodes were implanted simultaneously with subdural grids and/or strips, depth electrodes positions were adjusted following the procedure described by Taimouri et al. [14]. Briefly, using the projection of the subcortical electrodes on the cortical surface, it is possible to estimate the deformation field suffered by the brain due to the implant and apply a weighted displacement also on the depth electrodes (Fig. 1C).

D. Spikes detection and selection of spike propagations

Automatic detection of IEDs was performed through an in-house detector, developed in MATLAB®, for each channel individually. The detection was performed on the icEEG signal filtered between 1-70 Hz in standard average montage. Our detector selects peaks on the signal's derivative with prominence greater than a selected threshold (5-10 std for optimal spikes identification). Once selected, the closer local maximum/minimum of the original signal is identified as a spike. If more than one spike falls within a 10 ms window, only the one with the maximum value of electrical potential is selected. The spike detection was validated through visual inspection by M.M.

IEDs were categorized to define their spatiotemporal propagation with an automated algorithm able to delineate sequences of IEDs arising in neighboring electrodes, similarly to what we used in our previous studies [4], [15]. We discriminate the IEDs sequences in two different groups: (i) *propagation events*, if the IEDs sequences involved at least three IEDs originated by near channels, or (ii) *isolated-IEDs*. We defined a *propagation event* if: (i) the minimum number of channels was equal to 3; (ii) the maximum number of channels involved was less than 75% of the total electrodes; (iii) the time between two consecutive groups was at least 300 ms and (iv) the total duration was less than 5 standard deviations with respect to the mean. For the purposes of this study, isolated IEDs were discarded and only the first IED (*spike's onset*) of each propagation was considered for further analysis.

E. Forward Model

We extracted the cortical surface from the pre-operative MRI of each patient through *FreeSurfer* and calculated a realistic head model using the OpenMEEG software [16]. The realistic volumetric boundary model (BEM) of the sources was calculated using only the inner skull layer and only the hemisphere where the electrodes were implanted (Fig. 2A). When electrodes were implanted in both hemispheres, the BEM model was calculated including the entire brain. To acquire a more accurate model, an adaptive integration grid was used, with 17 layers from the cortical surface, a downsampling factor equal to 3 or 5 respectively for a single hemisphere or both, and an initial number of vertices equal to 4,000.

F. Electric Source Imaging of spike propagations

To obtain an estimation of the spatiotemporal brain activity, we used the dynamic Statistical Parametric Maps [17], how it is implemented in *Brainstorm*. For noise covariance, we used an identity matrix and computed the data covariance from all the windows centered around each spike's onset with a length of 200 ms. We calculated the spatiotemporal activity of spike propagations only for the events in time windows with a duration of 500 ms [from −200 to 300 ms, with 0 corresponds to the first onset spike] (Fig. 2B) with a correlation >0.7 between the reconstructed and the original signal. We then averaged in space all unconstrained maps of source activity (considering absolute values) to have a single global spatial map for each patient. In this overall average spatiotemporal map [3*N×M] (where N is the number of sources and M is the number of time samples), each source was modeled by three elementary dipoles placed in the three directions of the Cartesian MRI space. We then extracted the three components along the three axes of the current map for each temporal sample, and for each voxel we calculated the norm of the vector sum of the three spatial orientations. The final spatiotemporal map (S_{map} [N×M]) was then normalized with respect to the maximum value of activation: $S_{map} = \sqrt{S_x^2 + S_y^2 + S_z^2} \Big/ \max\left(\sqrt{S_x^2 + S_y^2 + S_z^2}\right)$.

Starting from S_{map}, we defined a volumetric region of activation (VRA) every 5 ms by averaging the activation values within this window (Fig. 2C). In order to reduce spurious activations, we considered as the VRA only the voxels with a normalized activation value greater than 70% based on the specific patient's S_{map} [18].

G. Comparison with Resection and SOZ

The temporal evolution of the VRAs allows us to define two zones: the ESI-onset zone and the ESI-spread zone. We defined these two zones by properly splitting the entire propagation, at time thresholds in the range 5-50% of the total duration time. Specifically, we defined as the ESI-onset zone the union of all the VRAs that occur before the threshold, and as ESI-spread zone, the union of VRAs that occur after the threshold (Fig. 2B). To quantify how these two zones can identify the EZ, we used the clinically defined SOZ and the resection zone as gold standards to estimate the EZ. Since all patients had good surgical outcome, the clinically defined SOZ and resection volume were proofs of successful delineation of the EZ. We, thus, evaluated the percentage of the volume of the ESI-onset zone and the ESI-spread zone that overlaps with the resection. We also computed the mean distances of the ESI-onset zone and ESI-spread zone both from resection and SOZ. Resection volume was obtained by manual co-registration of the pre- and post-operative MRI. The SOZ was defined by the clinicians as the icEEG electrodes where clinical seizures were initiated.

H. Statistical Analysis

Statistical analysis was performed with MATLAB. Volumes, overlapping volumes with resection and mean distances from resection and SOZ were compared between the ESI-onset and ESI-spread zone through Wilcoxon sign-rank test. Results are reported as median and IQR range and statistical significance was defined for $p < 0.05$.

III. Results

We observed spike propagation with ESI in all patients (9 [5.5-13.5] years, 4 males, number of icEEG: 98 [85-102]). From the spike detection and categorization, we found spikes across multiple icEEG channels in all patients and a number of propagation events equal to 149 [140-246.5]. For each patient, the number of VRAs analyzed was 30.5 [23.5-39].

We identified an optimal time threshold equal to 10% to define the ESI-Onset zone, based on a concurrent maximization of its overlap with resection and minimization of its distance from the resection. In addition, this percentage corresponds to a maximum time range of 30 ms, nicely in agreement with the temporal evolution of the spike onset (Fig. 4A-D), further validating our optimal selection from a clinical point of view.

Spike propagation had a mean duration of 155 ms [96-186 ms]. We found that the ESI-onset zone had a significantly smaller volume (more focal activity) compared to the ESI-spread zone (1.7 cm^3 [1.1-3.5 cm^3] vs. 28.3 cm^3 [7.2-74.3 cm^3]; $p = 0.02$) (Fig. 4E). We compared the ESI-onset and ESI-spread zones with respect to the resected volume (22.0 cm^3 [16.5-69.7 cm^3]) and the electrodes defined as SOZ (10.5 [4.5-22] electrodes). The volume percentage of the ESI-onset zone inside the resection was higher compared to the percentage for the ESI-spread zone (73.3 % [range: 47.4-100 %], 36.5 % [range: 20.3-59.9 %], $p = 0.008$) (Fig. 4E). We also observed a shorter distance of the ESI-onset zone from the resection compared to the ESI-spread zone (4.3 mm [3.4-5.5 mm], 7.4 mm [6.0-20.6 mm], $p = 0.008$) and the same trend for the distance of the ESI-onset zone from the SOZ (compared to ESI-spread zone) (11.9 mm [7.2-15.1 mm], 20.6 mm [15.4-27.2 mm], $p = 0.02$) (Fig. 4E).

IV. Conclusion

In this study, we propose a new methodology for mapping the spatiotemporal propagation of IEDs (and delineate its onset) using distributed ESI applied on icEEG recordings bypassing the limited spatial resolution of icEEG. We showed that the ESI-onset zone is a reliable biomarker of the EZ (defined here by the SOZ and resection of patients with good surgical outcome) in contrast to the ESI-spread zone. This notion is based on our observation that the ESI-onset zone overlaps with the resection zone (more than 50%) and has a significant shorter distance to the SOZ for patients with good surgical outcome (compared to the ESI-spread zone). Moreover, this ESI-onset zone is more focal than the areas of spread and thus it is less possible to overlap with eloquent areas of the brain whose removal is unnecessary and should be avoided during resective surgery. Our findings also reveal information about the pathophysiological mechanisms of IEDs propagation, which are specific to each patient since the propagation duration, and thus the number of VRAs in each propagation event, differs significantly from patient to patient. To better understand this phenomenon, future directions of this project aim to correlate the functional mapping of the IEDs propagation with structural information derived from diffusion imaging.

Acknowledgment

This work was supported by the National Institute of Neurological Disorders & Stroke 454 (RO1NS104116-01A1, PI: C. Papadelis; 1R21NS101373-01A1, PIs: C. Papadelis & S. Stufflebeam), and Cook Children’s Health

Foundation. A. Loppini and S. Filippi acknowledge the support of the National Group for Mathematical Physics (GNFM-INdAM).

References

[1]. Lüders HO, Najm I, Nair D, Widdess-Walsh P, and Bingman W, "The epileptogenic zone: General principles," Epileptic Disord, vol. 8, no. SUPPL. 2, pp. 1–9, 2006.

[2]. Rathore C and Radhakrishnan K, "Concept of epilepsy surgery and presurgical evaluation," Epileptic Disord, vol. 17, no. 1, pp. 19–31, 2015, doi: 10.1684/epd.2014.0720. [PubMed: 25652945]

[3]. Tamilia E, Madsen JR, Grant PE, Pearl PL, and Papadelis C, "Current and Emerging Potential of Magnetoencephalography in the Detection and Localization of High-Frequency Oscillations in Epilepsy," Front. Neurol, vol. 8, no. JAN, Jan. 2017, doi: 10.3389/fneur.2017.00014.

[4]. Tamilia E et al. , "Surgical resection of ripple onset predicts outcome in pediatric epilepsy," Ann. Neurol, vol. 84, no. 3, pp. 331–346, 2018, doi: 10.1002/ana.25295. [PubMed: 30022519]

[5]. Mălîia MD et al. , "Epileptiform discharge propagation: Analyzing spikes from the onset to the peak," Clin. Neurophysiol, vol. 127, no. 4, pp. 2127–2133, 2016, doi: 10.1016/j.clinph.2015.12.021. [PubMed: 26818882]

[6]. Tomlinson SB, Bermudez C, Conley C, Brown MW, Porter BE, and Marsh ED, "Spatiotemporal mapping of interictal spike propagation: A novel methodology applied to pediatric intracranial eeg recordings," Front. Neurol, vol. 7, no. DEC, pp. 1–12, 2016, doi: 10.3389/fneur.2016.00229. [PubMed: 26834696]

[7]. Tanaka N et al. , "Propagation of epileptic spikes reconstructed from spatiotemporal magnetoencephalographic and electroencephalographic source analysis," Neuroimage, vol. 50, no. 1, pp. 217–222, 2010, doi: 10.1016/j.neuroimage.2009.12.033. [PubMed: 20006721]

[8]. Papadelis C et al. , "Magnetoencephalographic Spike Analysis in Patients With Focal Cortical Dysplasia: What Defines a 'Dipole Cluster'?," Clin. Neurophysiol, vol. 83, no. 3, pp. 25–31, Jan. 2018, doi: 10.1016/j.pediatmeurol.2018.03.004.

[9]. Tamilia E et al. , "Assessing the localization accuracy and clinical utility of electric and magnetic source imaging in children with epilepsy," Clin Neurophysiol., vol. 130, no. 4, pp. 491–504, 2019, doi: 10.1016/j.clinph.2019.01.009. [PubMed: 30771726]

[10]. Alhilani M et al. , "Ictal and interictal source imaging on intracranial EEG predicts epilepsy surgery outcome in children with focal cortical dysplasia," Clin. Neurophysiol, vol. 131, no. 3, pp. 734–743, 2020, doi: 10.1016/j.clinph.2019.12.408. [PubMed: 32007920]

[11]. Tadel F, Baillet S, Mosher JC, Pantazis D, and M R. Leahy, "Brainstorm: A User-Friendly Application for MIEG/EEG Analysis," Comput. Intell. Neurosci, vol. 2011, pp. 1–13, 2011, doi: 10.1155/2011/879716. [PubMed: 21837235]

[12]. Prabhu S and Mahomed N, "Imaging of intractable paediatric epilepsy," South African J. Radiol, vol. 19, no. 2, pp. 1–10, Dec. 2015, doi: 10.4102/sajr.v19i2.936.

[13]. de Mlacedo Rodrigues K et al. , "A FreeSurfer-compliant consistent manual segmentation of infant brains spanning the 0-2 year age range," Front. Hum. Neurosci, vol. 9, no. FEB, pp. 1–12, Feb. 2015, doi: 10.3389/fnhum.2015.00021. [PubMed: 25653611]

[14]. Taimouri V et al. , "Electrode localization for planning surgical resection of the epileptogenic zone in pediatric epilepsy," Int. J. Comput. Assist. Radiol. Surg, vol. 9, no. 1, pp. 91–105, Jan. 2014, doi: 10.1007/s11548-013-0915-6. [PubMed: 23793723]

[15]. Tamilia E, Matarrese M et al. , "Noninvasive Mapping of Ripple Onset Predicts Outcome in Epilepsy Surgery," Ann. Neurol, pp. 1–15, 2021, doi: 10.1002/ana.26066.

[16]. Gramfort Alexandre, Papadopoulo Théodore, Olivi Emmanuel, and Clerc Maureen, "OpenMEEG: opensource software for quasistatic bioelectromagnetics," Biomed. Eng. Online, vol. 8, no. 1, p. 1, 2009, doi: 10.1186/1475-925X-8-1. [PubMed: 19138401]

[17]. M A. Dale et al. , "Dynamic statistical parametric mapping: Combining fMRI and MIEG for high-resolution imaging of cortical activity," Neuron, vol. 26, no. 1, pp. 55–67, 2000, doi: 10.1016/S0896-6273(00)81138-1. [PubMed: 10798392]

[18]. Pellegrino G et al. , “Accuracy and spatial properties of distributed magnetic source imaging techniques in the investigation of focal epilepsy patients,” Hum. Brain Mapp, vol. 41, no. 11, pp. 3019–3033, 2020, doi: 10.1002/hbm.24994. [PubMed: 32386115]

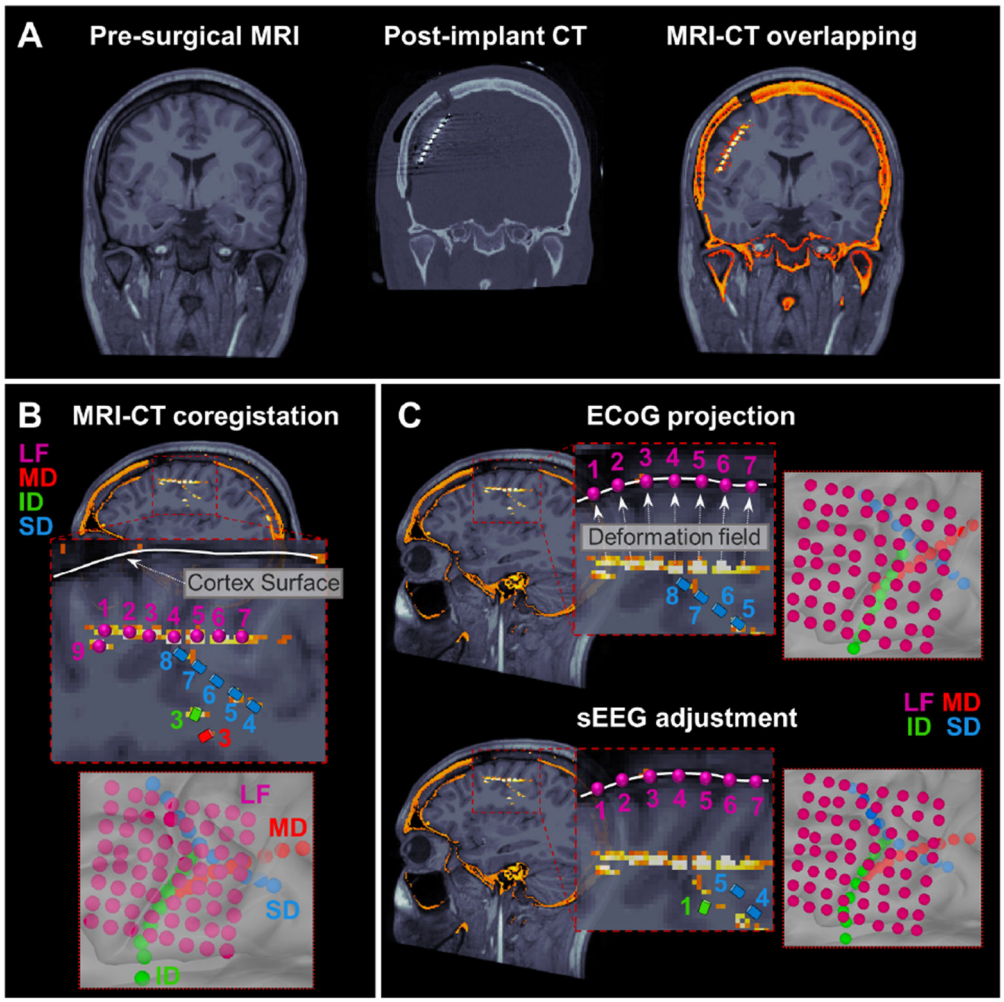

Figure 1. Pre-operative MRI and post-implant CT coregistration to obtain icEEG electrodes locations.

(A) Coronal view of pre-operative MRI, post-implant CT and overlapping MRI-CT scans for a 4-years old boy with 138 (108 ECoG and 30 sEEG) electrodes implanted. **(B)** MRI-CT coregistration process with focus on 8 ECoG electrodes (LF) and 7 sEEG electrodes (SD, MD, ID). **(C)** Brain shift correction with a two-step procedure: (i) ECoG electrodes were projected on the nearer cortical surface vertex, (ii) once the brain deformation field was estimated by the ECoG shifting, the weighted shift was also applied on sEEG electrodes.

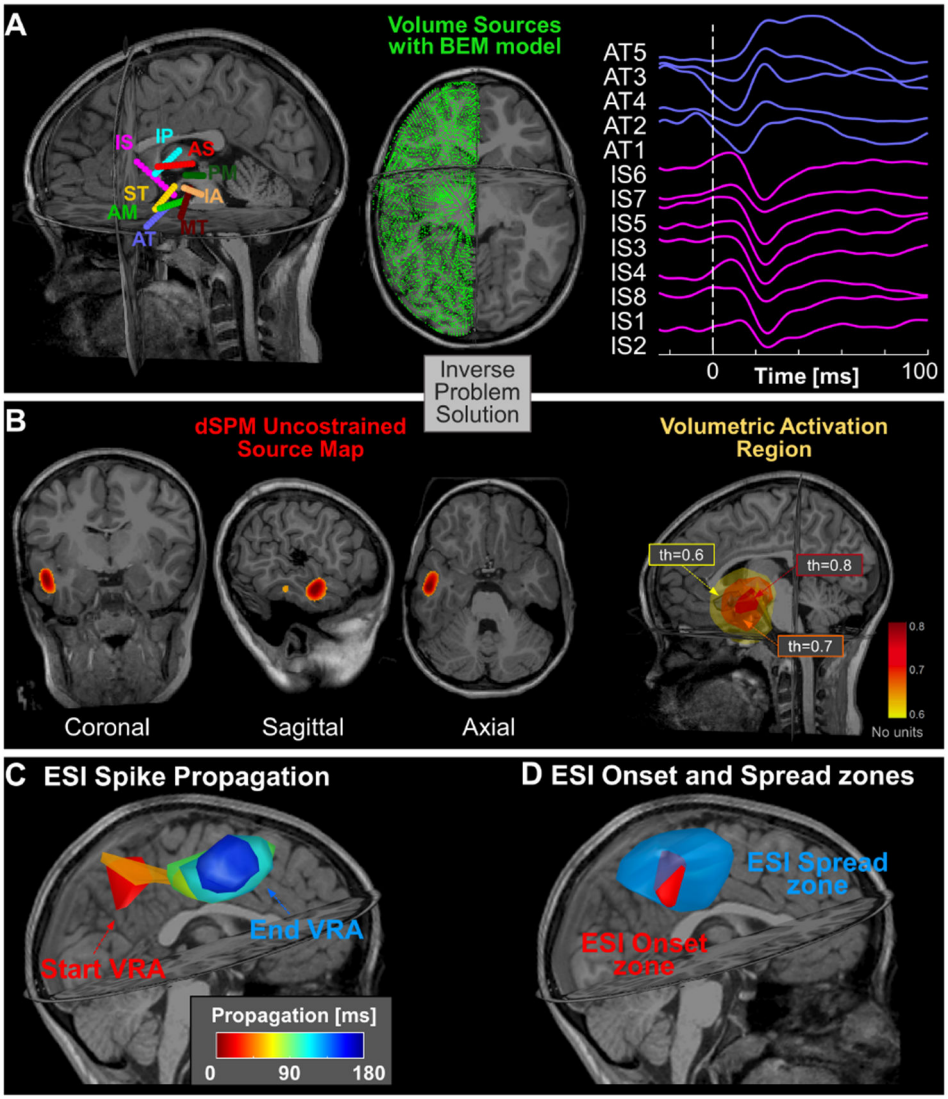

Figure 2. Electric Source Imaging on icEEG with dSPM.

(A) Locations of icEEG leads with respect to patient's MRI (patient #2) (left); volume grid estimated through BEM modeling for solving the forward problem (middle); icEEG recordings showing a spike propagation event in two of the icEEG leads (AT & IS) (right). **(B)** A VRA estimated through the dSPM at one time point (left). The VRA for different thresholds: th = 0.6, 0.7, and 0.8. **(C)** VRA propagation created every 5 ms by averaging the activation values (above 70%) in that window (patient # 3); **(D)** ESI-onset zone definition as the VRA given by the union of all the VRAs within the first 10% of the entire duration of propagation phenomenon and ESI-spread zone definition as the VRA given by the union of all the VRAs that occur at the remaining 90% of propagation.

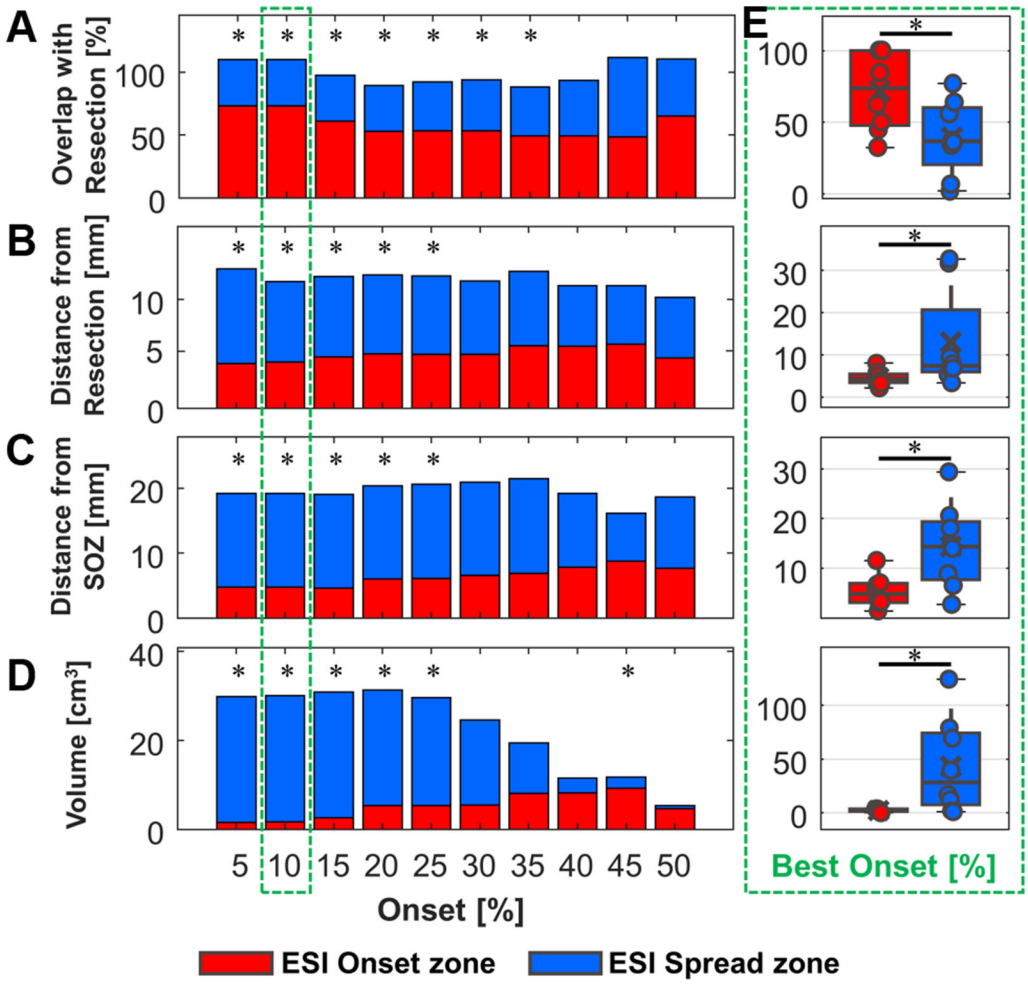

Figure 3. Comparison between ESI-onset zone and ESI-spread zone.

(A) The median overlap of the ESI-onset and ESI-spread zones inside resection for different percentage of onset. **(B)** The median distance of the ESI-onset and ESI-spread zones from resection. **(C)** The median distance of the ESI-onset and ESI-spread zones from the SOZ. **(D)** Median volume of ESI-onset zone compared with ESI-spread zone. **(E)** Boxplots for all the previous metrices with the optimal onset percentage. (The stacked bar plots report only the median value excluding information about IQR. In all the panels * indicates $p < 0.05$ for paired Wilcoxon sign-rank test).

TABLE I.

Demographics

ID #	Age[y]	Sex	iEEG [#]	Side	MRI Finding	# SOZ elect.	Res. Vol. [cm^3]
1	10	M	EC [80]	R	Norm	4	16.4
2	7	F	sE [90]	L	FCD (T,Ins)	6	16.5
3	8	F	EC+sE [80+20]	R(Inter)	FCD (P)	23	25.8
4	14	F	EC [72]	L(Inter)	FCD (P)	2	9.4
5	3	M	EC [96]	L	FCD (Fr)	5	54.0
6	13	M	EC+sE [72+30]	L	ENE (P,T)	21	22.2
7	4	M	EC+sE [108+30]	R(Both)	FCD (Fr)	35	84.3
8	14	M	sE [102]	R	FCD (P)	15	10.8

M: Male, F: Female, R: Right, L: Left, Inter: interhemispheric, EC: ECoG, sE: sEEG, FCD: Focal Cortical Dysplasia, ENE: Encephalomalacia, T: Temporal, Ins: Insula, P: Parietal, Fr: Frontal.